



Asymmetric structure and non-linear transition behaviour of the wakes of toroidal bodies

Gregory John Sheard*, Mark Christopher Thompson, Kerry Hourigan

Fluid Dynamics Laboratory for Aeronautical and Industrial Research (FLAIR), Department of Mechanical Engineering, Monash University, Clayton, Victoria, 3800 Australia

Received 31 March 2003; accepted 14 April 2003

Abstract

The flow past three different aspect ratio toroids is studied numerically to elucidate the various non-axisymmetric wake transition modes previously predicted by linear stability analysis. The transitions are modelled with respect to the Landau equation, and the criticality of the various transitions is determined from the coefficients of the Landau equation.

The wake flow fields are simulated using a spectral-element scheme, incorporating a Fourier expansion of the two-dimensional grids in the azimuthal direction to evolve the three-dimensional wake flow.

Linear Floquet stability analysis performed previously on the wakes of bluff rings has predicted a series of non-axisymmetric transitions at various aspect ratios. Bluff rings with smaller aspect ratios (those approaching the sphere geometry) are predicted to undergo a regular asymmetric transition (i.e., steady to steady flow), followed by a Hopf bifurcation to an unsteady wake with increasing Reynolds number. Three transition modes have been identified in this aspect ratio range, referred to as modes I, II and III, respective to increasing aspect ratio.

Tracer particle and iso-surface plots visualizing the aforementioned transition modes are provided, which reveal the details of the wake structure associated with the saturated modes.

© 2003 Elsevier SAS. All rights reserved.

Keywords: Bluff body wakes; Landau equation; Three-dimensional wake transition; Flow visualisation; Regular transition; Hopf transition

1. Introduction

The various transitions in the wake of bluff rings, or toroids, have been studied over the past decade [1–3] with a rich diversity of wake states being determined. The bluff ring geometry is of interest as a fundamental bluff body due to its inherent characteristic whereby the adjustment of a single geometric parameter (the aspect ratio, Ar) allows a wide range of geometry to be represented. By varying the single geometric parameter Ar , a uniform axisymmetric body is described varying from a sphere at $Ar = 0$, to a straight cylinder at the limit $Ar \rightarrow \infty$. Fig. 1 shows a schematic diagram of the bluff ring system.

This paper studies aspect ratios in the range $0 \leq Ar \leq 4$. It has been predicted from linear stability analysis [2] that three distinct three-dimensional transition modes exist over this range of aspect ratios, as shown in Fig. 3.

Aspect ratios $Ar = 0.6$, 1.6 and 2.0 are chosen to isolate each of the three asymmetric transition modes identified in previous work (mode I, II and III transitions respectively). Asymmetric numerical computations employing a spectral-element method with an azimuthal Fourier expansion (see [4,5] for a description of the numerical method, and [2,3] for grid resolution studies) are used to compute the asymmetric wakes arising from these transitions. The Reynolds number length scale is based on the diameter d .

* Corresponding author.

E-mail address: Greg.Sheard@eng.monash.edu.au (G.J. Sheard).

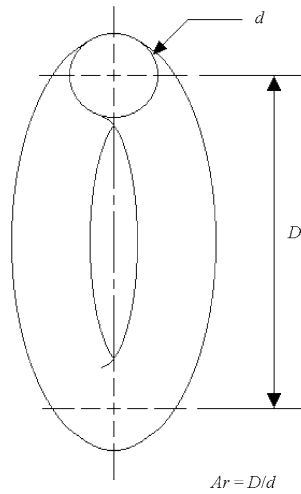
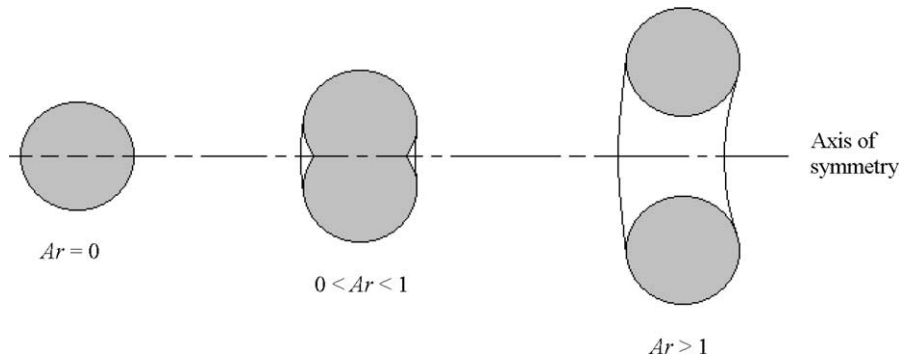


Fig. 1. Schematic diagram of the bluff ring system.

Fig. 2. Cross-section views of three aspect ratio cases that are pertinent to the present study. A sphere ($Ar = 0$) is shown at the left, the centre shows a solid ring (i.e., no hole on the axis), and the right shows a ring with a hole on the axis.

The Landau equation is used to determine whether the non-axisymmetric transitions are supercritical or subcritical. In the Landau equation the growth of the unstable mode is described by a differential equation for the complex amplitude (A) of the unstable mode that varies in time (t):

$$\frac{dA}{dt} = (\sigma + i\omega)A - l(1 + ic)|A|^2A + \dots \quad (1)$$

The standard treatment of the Landau equation is applied through a decomposition into real and imaginary parts (e.g., Le Gal et al. [6]). By assuming that the saturated amplitude takes the form $A = \rho \exp(i\Phi)$, where ρ and Φ are real variables for the magnitude and phase angle of the amplitude, respectively, the cubic truncation of the Landau equation can be decomposed into Eqs. (2) and (3).

$$\frac{d \log(\rho)}{dt} = \sigma - l\rho^2 = 0 \quad \text{at saturation,} \quad (2)$$

$$\frac{d\Phi}{dt} = \omega - lc\rho^2 = \omega_{\text{sat}} \quad \text{at saturation.} \quad (3)$$

For regular transitions phase information is neglected, and the non-linear behaviour is determined from the sign of the l -term in Eq. (2). For Hopf bifurcations, phase information is considered, and application of Eq. (3) allows further transition properties to be ascertained. A positive value of l allows the cubic term in Eq. (2) to cause saturation of the transition, and such transitions are said to occur through a supercritical bifurcation. Supercritical transitions do not exhibit any hysteresis in the vicinity of the critical Reynolds number for the transition. A negative l -value requires quintic or higher-order amplitude terms to be included in the truncation. These transitions occur through a subcritical bifurcation, with multi-valued solutions for the

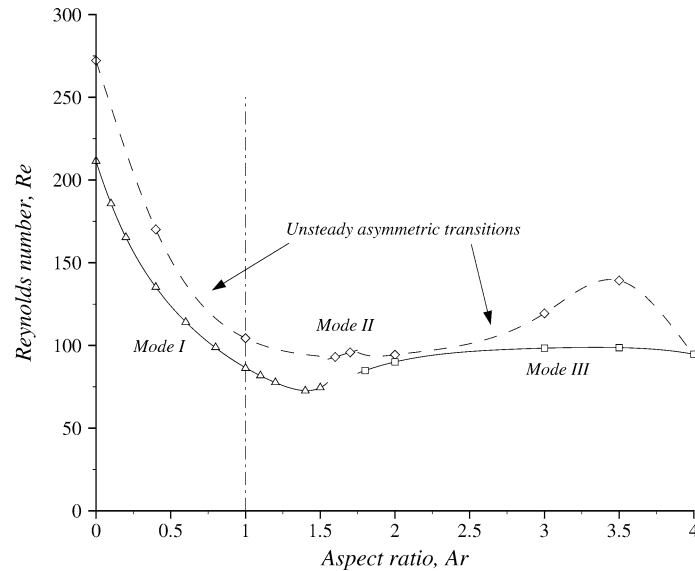


Fig. 3. Plot showing predicted critical transition Reynolds number profiles for dominant asymmetric stability modes in the wake of rings with aspect ratios $0 \leq Ar \leq 4$. The mode I, II and III transitions are represented by solid lines, with measured mode I and mode III values indicated by triangles and squares, respectively. Diamonds indicate the measured values of the critical Reynolds number for the Hopf transition in the wake, with dashed lines for the mode I and III aspect ratio ranges, and a solid line showing the mode II transition range. The dotted line at $Ar = 1$ marks the transition aspect ratio at which the hole through the center of the ring first emerges.

amplitude being described in the vicinity of the transition. Subcritical transitions exhibit hysteretic behaviour in the vicinity of the critical Reynolds number of the transition.

To determine the nature of the transition, the azimuthal velocity signal is monitored at a point in the wake. This “point method” has been applied by Dušek et al. [7] and Thompson et al. [5], and is applied in the present study. It relies on the assumption that at any point in the near wake the transition behaviour will approximately represent the global behaviour of the flow field.

2. Results I. Visualising the small aspect ratio 3D transition mode wakes

In this section, the non-axisymmetric wake structures that evolve following the regular mode I and III transitions, and the Hopf mode II transition are investigated. The saturated non-axisymmetric wakes that evolve at Reynolds numbers greater than the critical Reynolds numbers of the mode I, II and III transitions are represented by streamwise vorticity isosurface plots in Fig. 4.

It is clear from the isosurfaces plots in Fig. 4 that a plane of symmetry exists in the wakes through the centre of the ring for all modes. This symmetry has been observed for the sphere [8,9], which is another example of the mode I transition. Note that an $m = 1$ azimuthal symmetry maintained for each mode, as predicted by linear stability analysis [2]. In Fig. 4(a), wings of streamwise vorticity located immediately behind the ring are observed, as is a pair of tails of vorticity stretching far downstream. These structures are indicative of the classic “double threaded wake” observed in the wake of the sphere [8,5] following the first asymmetric transition.

The near wake following the mode II transition (Fig. 4(b)) is similar to the mode I near wake region, with wings of streamwise vorticity of opposing sign wrapped around longer tails of streamwise vorticity extending downstream. Here, these tails are not steady in time, instead they are shed downstream. The mode II transition is a Hopf transition from a steady axisymmetric flow to an asymmetric unsteady flow. This verifies the predictions of Sheard et al. [2], that the dominant linear transition mode is oscillatory, resulting from a Hopf transition to an unsteady asymmetric wake.

The wake of the ring following the mode III transition is shown in Fig. 4(c). This mode is a regular (steady-steady) transition to asymmetry, as is mode I. Structurally the wake differs significantly from the mode I transition wake. Clearly, the absence of asymmetrical vortical structures extending far downstream along the axis indicates that the mode III wake is fundamentally different to the mode I wake. The non-axisymmetric structures are localised within approximately $5d$ of the body, and are situated directly downstream of the ring cross-section. The location of the non-axisymmetric structures indicates that the mode

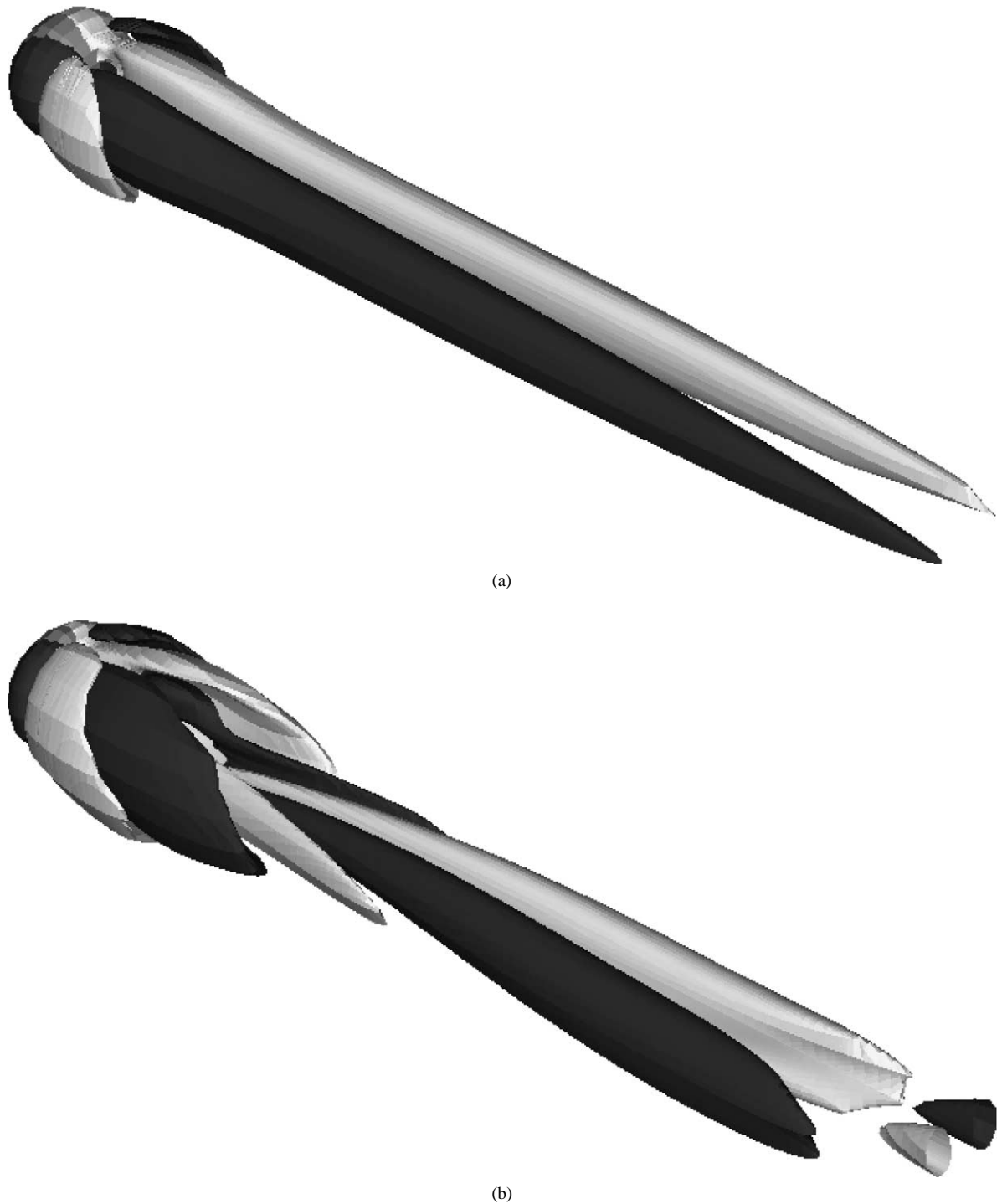
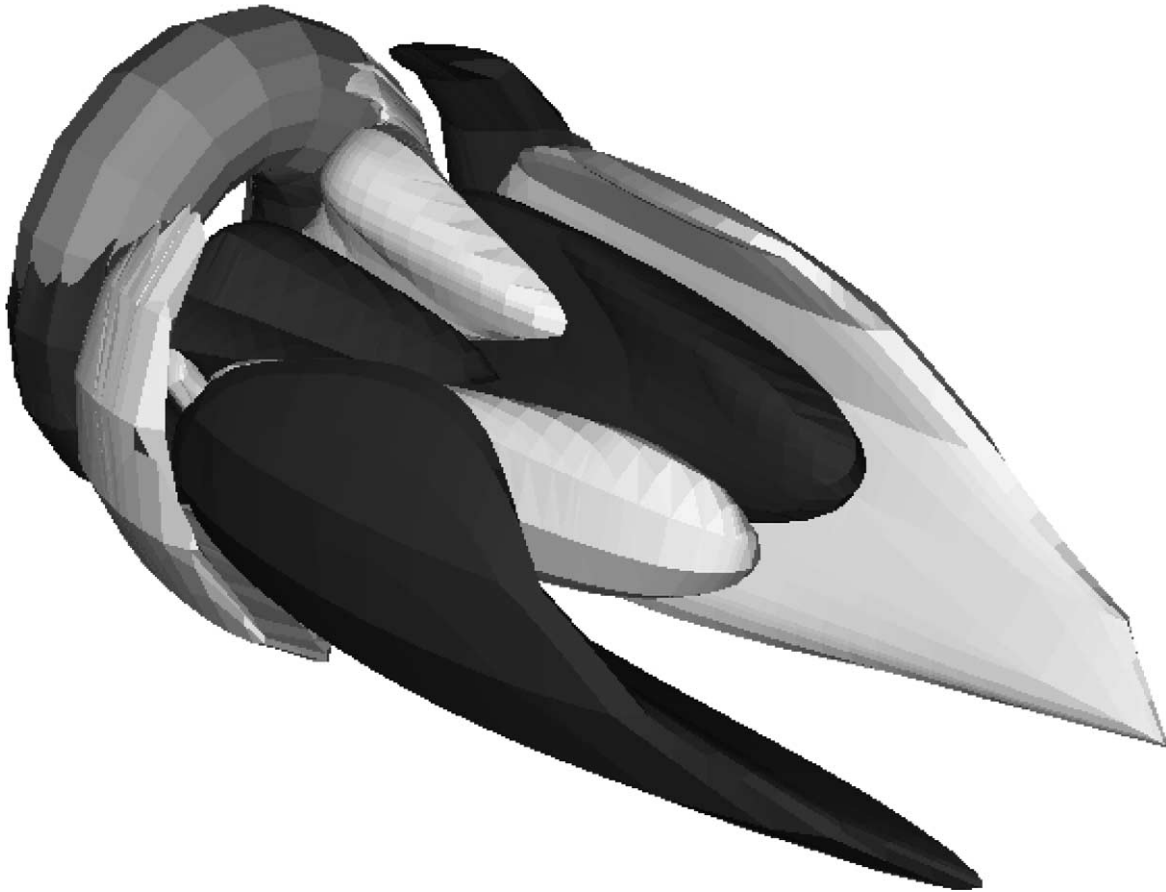


Fig. 4. Isosurface plots of streamwise vorticity indicating the asymmetric wake structures for bluff ring wakes following the mode I, II and III transitions. The mode I wake for the $Ar = 0.6$ ring at $Re = 130$ is shown in part (a), the mode II wake for the $Ar = 1.6$ ring at $Re = 100$ is shown in part (b), and the mode III wake for the $Ar = 2.0$ ring at $Re = 100$ is shown in part (c). Light grey isosurfaces represent positive streamwise vorticity, and dark grey isosurfaces represent negative streamwise vorticity. The bluff ring body is located at the upper left corner of each frame, and the flow direction is from the top left to the bottom right in each case.



(c)

Fig. 4. Continued.

III transition involves a loss of azimuthal stability of the recirculation region behind the ring cross-section, rather than a recirculation region at the axis as occurs for the mode I transition. This agrees with the stability analysis results of Sheard et al. [2].

3. Results II. Landau modelling of the mode I and III asymmetric transitions

The non-linear behaviour of the regular mode I and mode III transitions is studied by determining the Landau coefficients for an azimuthal velocity transient at a point displaced radially from the axis, and positioned $4d$ directly downstream of the cross-section of each ring. The criticality of each mode is determined, and where applicable comparisons are drawn with previous work on sphere stability [5] and bluff rings [2]. The mode II Hopf transition, and the Hopf transitions following the regular mode I and mode III transitions are studied later.

3.1. The mode I transition

The mode I transition has been found to be supercritical for the $Ar = 0.6$ ring, in agreement with Ghidersa and Dušek [10], and Thompson et al. [5], who determined that the regular asymmetric transition of the wake of a sphere (a geometry in the mode I aspect ratio regime) is supercritical. The plots in Fig. 5 illustrate the supercritical behaviour.

The critical Reynolds number for the mode I transition was determined from the growth rate (σ) from the Landau model. The resulting critical Reynolds numbers matched those predicted by the linear Floquet stability analysis of Sheard et al. [2] to within 0.5%; with $Re_c = 114$ for the $Ar = 0.6$ ring being found.

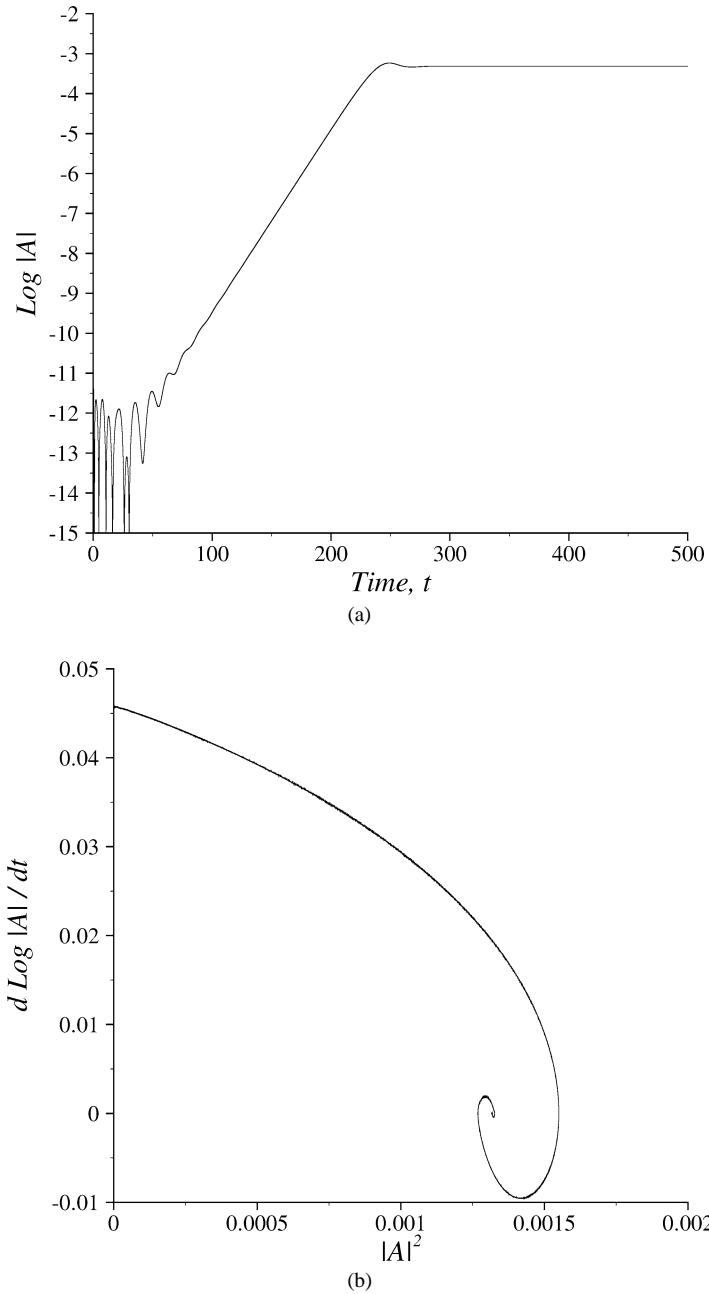


Fig. 5. Part (a) shows the evolution of the asymmetric transient in the wake of the $Ar = 0.6$ ring at $Re = 130$. Part (b) shows the amplitude derivative versus amplitude squared plot. The y-axis intercept gives growth rate (σ), and the gradient close to y-axis provides the saturation term, l . The negative slope and linear behaviour near the y-axis indicate that the transition is supercritical.

3.2. The mode III transition

The mode III transition is a regular transition, whereby the steady axisymmetric wake bifurcates to a steady asymmetric wake. Landau modelling of the non-linear behaviour of the transition shows it to be subcritical. The behaviour of this transition for a ring with $Ar = 2$ at $Re = 98$ is shown in Fig. 6. Fig. 6(b) shows subcritical behaviour, with a positive gradient at the y-intercept and a distinctly non-linear profile. Thus higher order terms are required for the Landau equation to adequately model the growth of the transition to saturation.

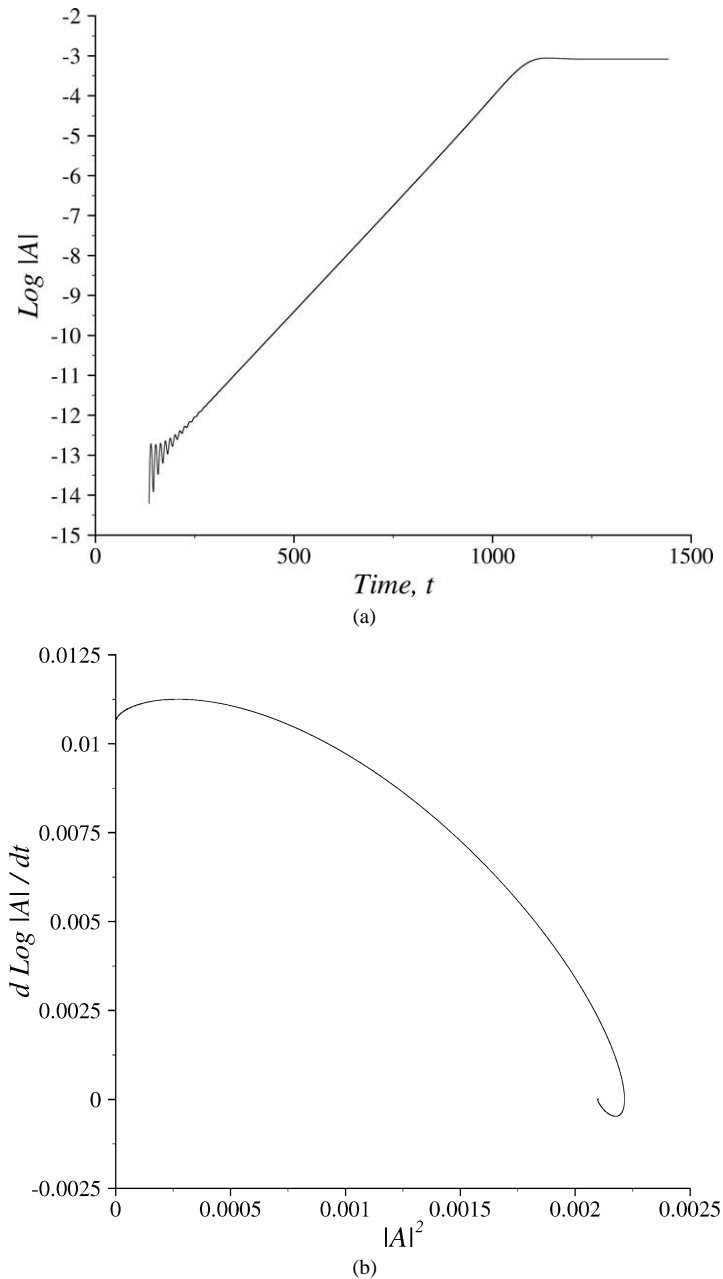


Fig. 6. Part (a) shows the evolution of an asymmetric transient in the wake of a $Ar = 2$ ring at $Re = 98$. Part (b) shows the amplitude derivative versus amplitude squared plot. The y-axis intercept gives growth rate (σ) and the gradient at the y-axis provides the saturation term, l . The positive gradient and non-linear profile in the vicinity of the y-axis indicate that the transition is subcritical.

4. Results III. Visualising the hopf transition modes of small aspect ratio ring wakes

This section provides visualisations of the vortical structure of the unsteady wakes computed at Reynolds numbers greater than the critical Reynolds number of the Hopf transitions in the aspect ratio ranges of the mode I, II and III transitions. Iso-surfaces are plotted using the method of Jeong and Hussain [11] to capture the non-axisymmetric vortical structures present in the wakes.

The regular mode I and mode III transitions are followed by a secondary Hopf transition to an unsteady asymmetric wake flow at higher Reynolds numbers. For a sphere wake this transition occurs at $Re = 272$ [9,5], and the resulting wake

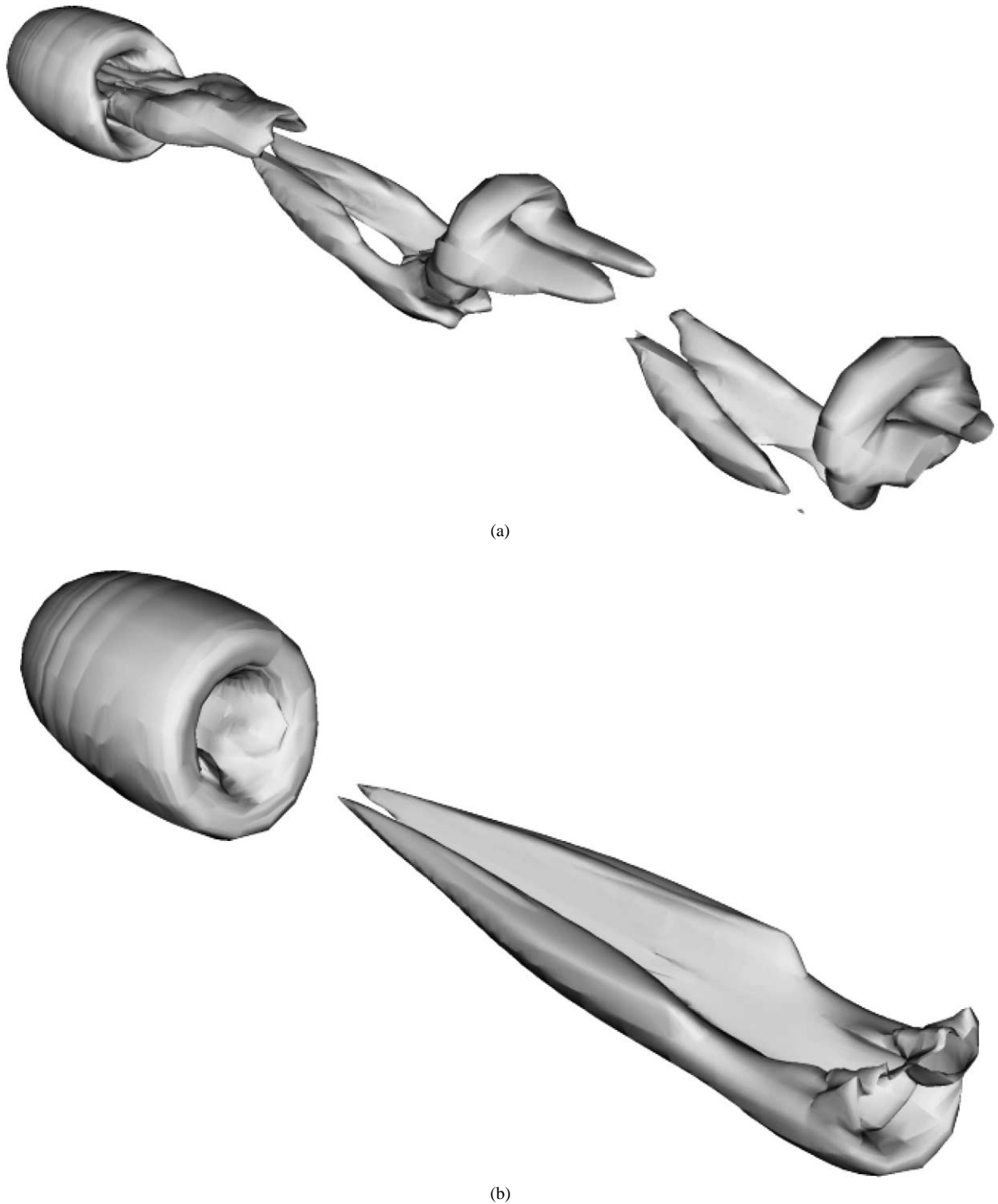
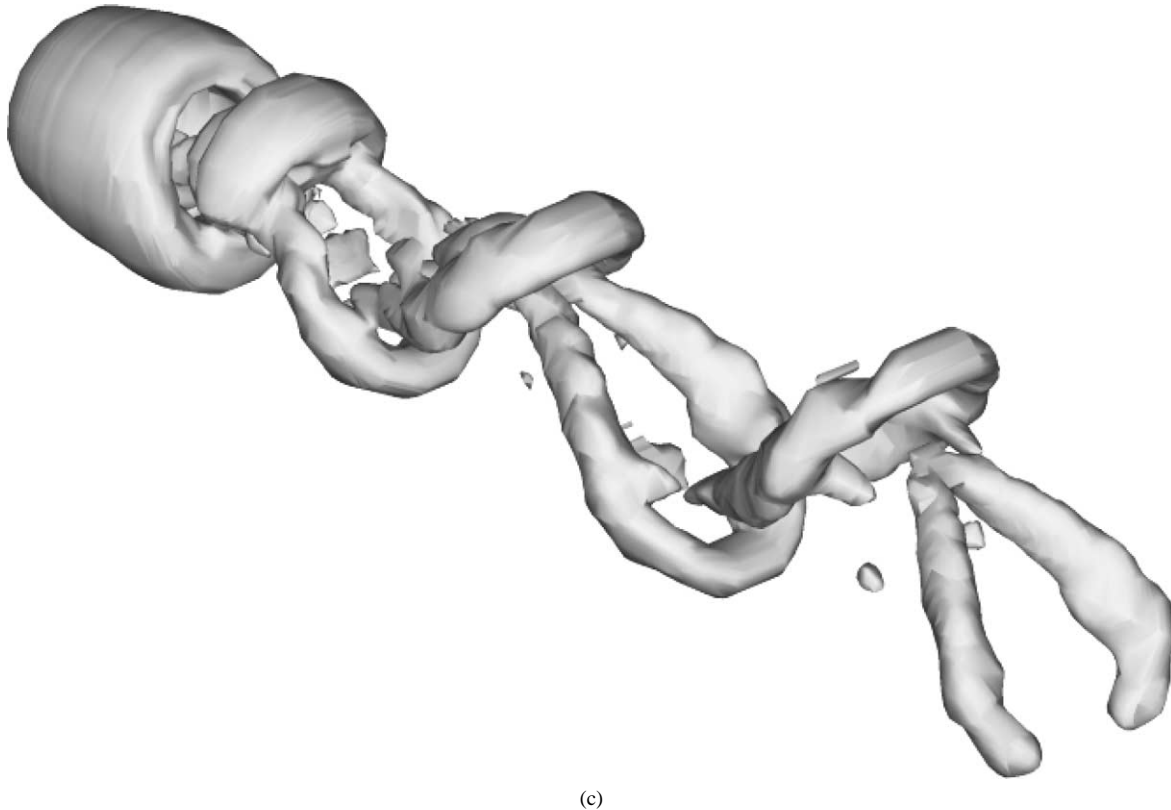


Fig. 7. Vortical iso-surface plots elucidating the wake structure of the bluff rings at Reynolds numbers above the Hopf transitions in the mode I, mode II and mode III aspect ratio ranges. The wake following the Hopf transition in the mode I transition aspect ratio regime is shown in part (a) for the $Ar = 0.6$ ring at $Re = 160$. The mode II Hopf transition wake is shown in part (b) for the $Ar = 1.6$ ring at $Re = 100$. The wake following the Hopf transition in the mode III aspect ratio regime is shown in part (c) for the $Ar = 2.0$ ring at $Re = 150$. Note the plane of symmetry through centre of each ring, and the similar hairpin-type vortical structure of the wakes. Flow is from top left to bottom right in each frame.



(c)

Fig. 7. Continued.

is characterised by a plane of symmetry along the axis, and an azimuthal symmetry $m = 1$. The wake structure consists of hairpin shaped vortex loops shedding alternately from opposite sides of the axis. The plots in Fig. 7 show similar “hairpin” structures in the wakes of both an $Ar = 0.6$ and an $Ar = 2.0$ ring subsequent to the mode I and mode III transitions. An $m = 1$ azimuthal symmetry is observed for each of the wakes presented here, and a plane of symmetry exists along the axis in each case.

The mode II wake (in Fig. 7(b)) differs from the wakes in parts (a) and (c) in that the Strouhal frequency of the oscillation is not periodic, and the average Strouhal frequency obtained was also far lower (being approximately 30% of the Strouhal frequencies of the wakes in the mode I and mode III transition regimes). The vortical isosurfaces plot of the mode II wake has been obtained from the same velocity field as the streamwise vorticity plot in Fig. 7(b). The mode II wake differs from the classic hairpin wake in that long vortical folds are cast into the wake from one side of the axis only.

4.1. Symmetry characteristics of the mode III transition

Interestingly, the mode III transition wake undergoes an azimuthal symmetry-breaking phenomenon between $Ar = 2$ and $Ar = 3$, from an $m = 1$ to an $m = 2$ mode. The scaling characteristics of the mode III transition are discussed shortly, however it should be noted that the non-axisymmetric wake structures associated with the mode III transition appear to occur with an azimuthal length proportional to d . The change in symmetry is highlighted by the visualisations from particle trace computations presented in Figs. 8 and 9. The particle trace computations involved the simulated injection of particles into the saturated non-axisymmetric wake. The injection points were carefully chosen so that the particle motion would best mimic the entrainment of dye into the wake that one would observe experimentally. This was achieved by placing the injection points in the vicinity of the rear separation points around the ring cross-section, and near to the surface (raised approximately $0.04d$ from the ring surface).

Notice that the wake in Fig. 8 appears to adopt a similar hairpin structure to the unsteady sphere wake [9,5], and the small aspect ratio ring wakes in Fig. 7. In fact, the particle trace visualisation in Fig. 8 is produced from the same computation that provided the iso-surface plot in Fig. 7(c). In Fig. 9, the plan and profile views clearly indicate the $m = 2$ azimuthal symmetry, with two perpendicular planes of symmetry observed in the wake.

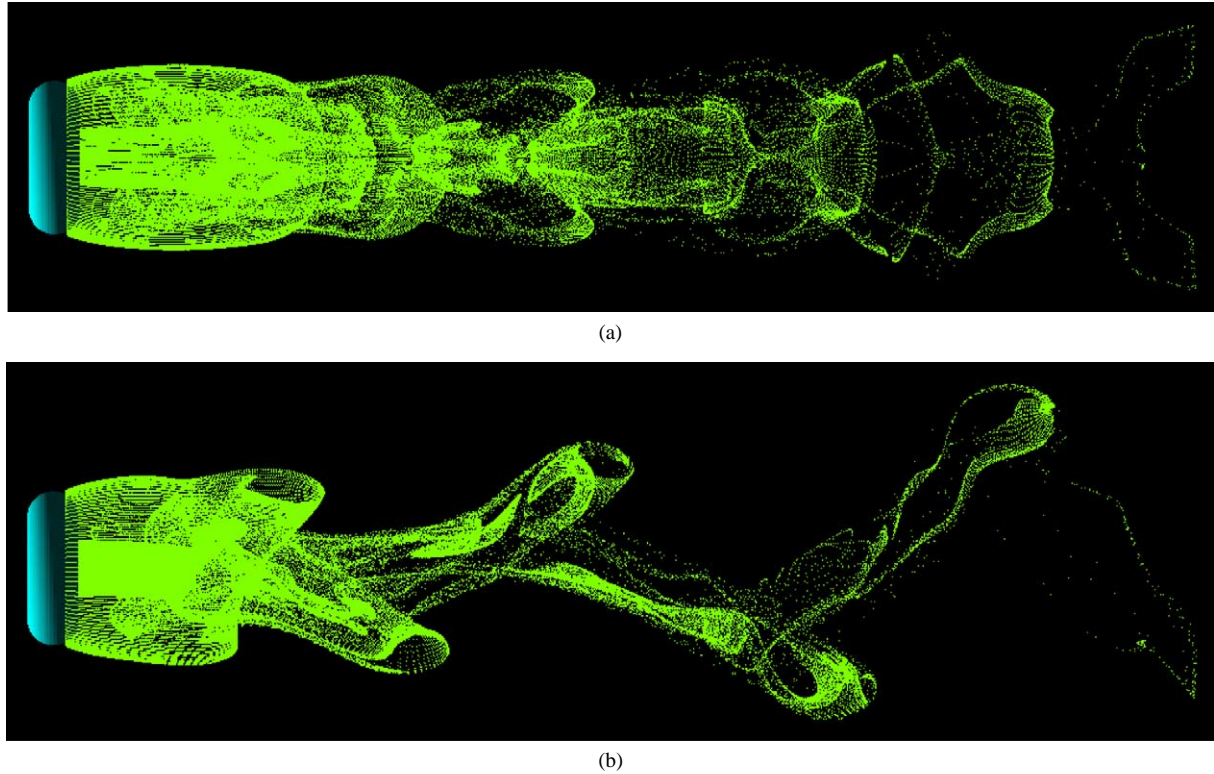


Fig. 8. Plan (a) and profile (b) views of the unsteady wake of the $Ar = 2$ ring at $Re = 150$, visualised from particle trace computations. Notice the azimuthal mode number $m = 1$ symmetry of the wake, and the similarity in wake structure to the classic unsteady sphere wake. In each frame the ring is located at the far left, and flow is from left to right.

The symmetry of the wakes of the $Ar = 2$ ring presented in Fig. 8, and the $Ar = 3$ ring presented in Fig. 9 may be quantified by the relationships of Eqs. (4) and (5), respectively. The period of oscillation of the wake is given by T , and the cylindrical polar coordinates are z , r and θ . The velocity fields of the $Ar = 2$ and $Ar = 3$ rings are given by $\mathbf{u}_{Ar=2}$ and $\mathbf{u}_{Ar=3}$, respectively.

$$\mathbf{u}_{Ar=2}(z, r, \theta, t) = \mathbf{u}_{Ar=2}(z, r, \theta + \pi, t + T/2), \quad (4)$$

$$\mathbf{u}_{Ar=3}(z, r, \theta, t) = \mathbf{u}_{Ar=3}(z, r, \theta + \pi/2, t + T/2). \quad (5)$$

By observing the location of the non-axisymmetric wake structures in Fig. 4(c), it is clear that the non-axisymmetric wake structures are located directly downstream of the cross-section of the ring. This indicates that the non-axisymmetric instability mode scales with the local recirculating wake region directly downstream of the ring cross-section, hence scaling with the cross-section diameter, d . This explains the increasing azimuthal mode number of the mode III transition wakes with aspect ratio, as the transition mode attempts to conform to a particular azimuthal wavelength proportional to d .

5. Results IV. Landau modelling of the hopf transitions for small aspect ratio rings

The non-linear behaviour of the Hopf transitions of bluff rings with aspect ratios in the range $0 \leq Ar < 4$ is examined by application of the Landau equation, and the results are summarised here.

5.1. Criticality of the Hopf transition modes

The Hopf transition following the mode I transition for the $Ar = 0.6$ ring is a supercritical Hopf transition. The mode II transition is found to occur through a supercritical bifurcation of the steady axisymmetric wake, resulting in an unsteady asymmetrical wake. The criticality of the Hopf transition that occurs in the wake of rings in the mode III transition aspect ratio regime is supercritical. It is interesting that the Hopf transition in the mode III transition regime is supercritical, as the regular mode III transition is subcritical.

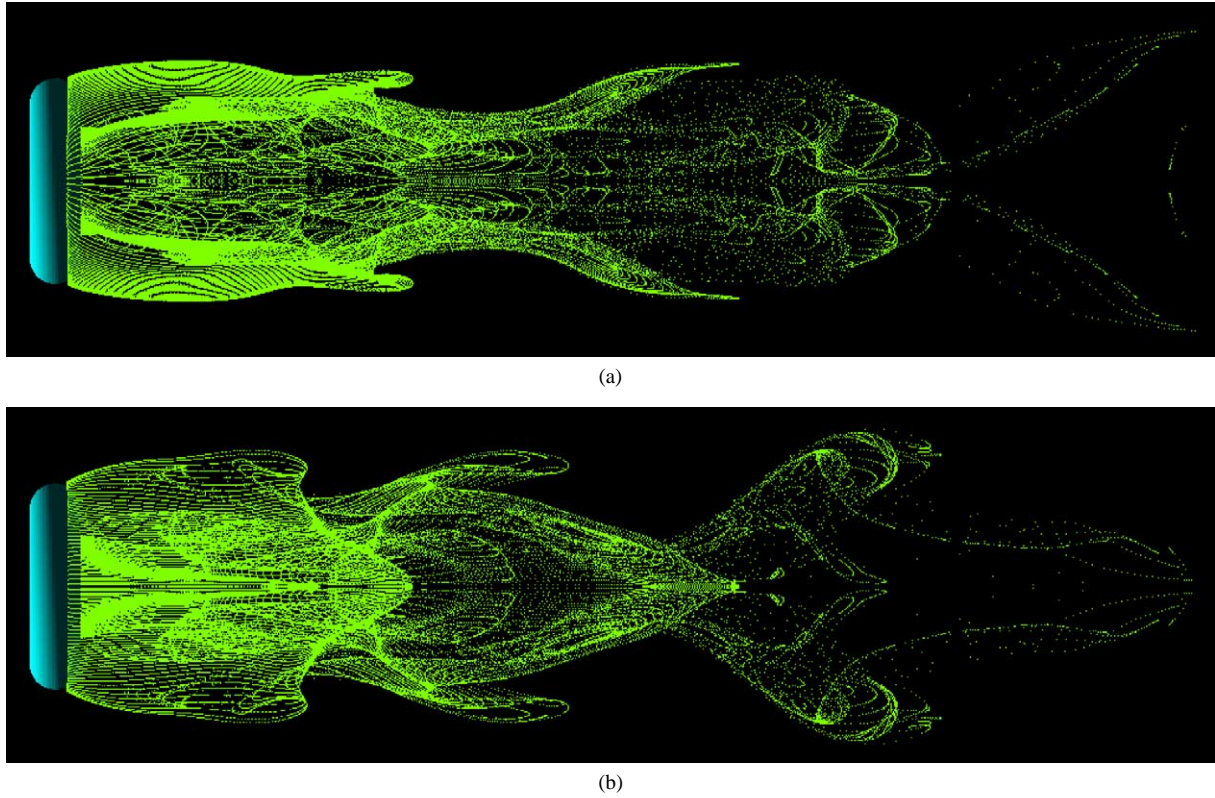


Fig. 9. Plan (a) and profile (b) views of the unsteady wake of the $Ar = 3$ ring at $Re = 138$, visualised from particle trace computations. Notice the azimuthal mode number $m = 2$ symmetry of the wake, observable as perpendicular planes of symmetry in parts (a) and (b). In each frame the ring is located at the far left, and flow is from left to right.

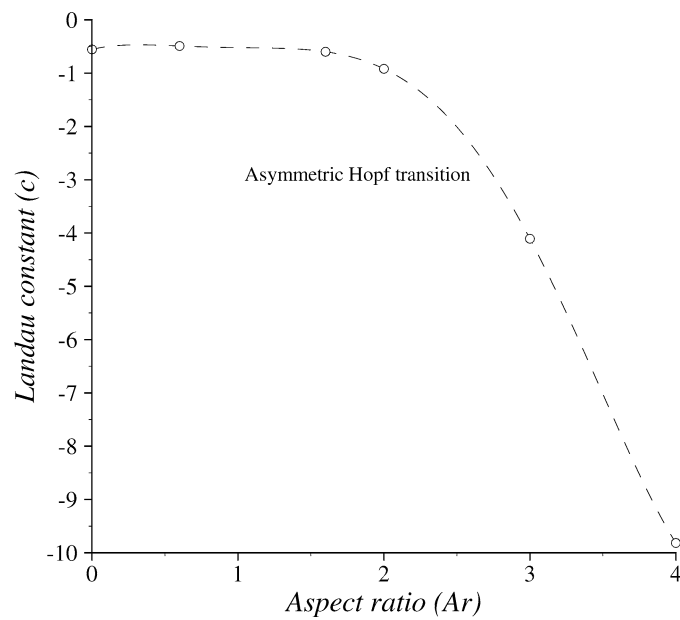


Fig. 10. Variation of measured Landau constant values with aspect ratio.

The consistent supercritical behaviour throughout the small aspect ratio ring range $0 \leq Ar < 4$ supports observations of the wake structures that indicate a similarity in vortical structure and hairpin-type shedding.

5.2. The Landau constant

The Landau constant in the complex Landau equation describes the shift in frequency between the linear growth regime of the instability, and the saturated regime. The Landau constant is a global parameter, and is defined by Eq. (6), which is obtained by combining Eqs. (2) and (3).

$$c = \frac{\omega - \omega_{\text{sat}}}{\sigma}. \quad (6)$$

In Eq. (6), σ is the growth rate of the instability, ω is the angular oscillation frequency of the mode in the linear growth regime, and ω_{sat} is the angular oscillation frequency of the instability mode once a saturated state has been reached. Fig. 10 shows the variation in the values of the measured Landau constants over the aspect ratio range $0 \leq Ar \leq 4$.

At $Ar = 0$, the measured Landau constant is in close agreement with the value of $c = -0.554$ measured by Ghidersa and Dušek [10] and Thompson et al. [5]. The measured Landau constants throughout the mode I aspect ratio range $0 \leq Ar < 1.6$ remain near to the Landau constant of the sphere wake. Interestingly, over the mode II and III aspect ratio range, the magnitude of the Landau constants grows significantly. At $Ar = 4$, the Landau constant $c = -9.9$, which is approximately 18 times the magnitude of the Landau constants measured over the mode I aspect ratio range.

6. Conclusions

Plots of streamwise vorticity, and iso-surface plots identifying the vortical structure of unsteady non-axisymmetric wakes have enabled the regular and Hopf transitions of bluff rings with $Ar < 4$ to be identified and characterised. The predicted existence and characteristics of three transition modes has been verified, with initial regular transitions to steady non-axisymmetric wakes occurring over the mode I and mode III transition regimes, followed by Hopf transitions with increasing Reynolds number. Furthermore, the predicted spontaneous Hopf transition to an unsteady non-axisymmetric wake was confirmed over the mode II transition regime.

By determining the Landau coefficients for the non-linear behaviour of azimuthal velocity transients in the wake of these bluff rings, the criticality of the various transitions has been determined. The regular mode I transition is found to be supercritical, as is the subsequent Hopf transition over the same aspect ratio range, in agreement with the previous studies of the sphere wake by Thompson et al. [5], in 2001. The mode II Hopf transition is found to occur through a supercritical bifurcation from a steady, axisymmetric wake, to an unsteady asymmetrical wake, in the absence of a regular asymmetrical transition. This corresponds to the linear Floquet stability analysis of Sheard et al. [2], in 2001. The mode III transition is found to be subcritical, while the subsequent Hopf transition over the same aspect ratio range is found to be supercritical. This leads to the conclusion that the hairpin wake scales with the ring diameter, D , rather than the ring cross-section diameter, d , of the regular mode III transition, and therefore is the same transition mode for aspect ratios over the mode I and mode III transition range.

The results of particle trace computations are presented to illustrate the azimuthal symmetry breaking in the mode III transition regime, between aspect ratios $Ar = 2$ and $Ar = 3$. The change in azimuthal mode number from $m = 1$ to $m = 2$ indicates that the wake in the mode III transition regime may in fact scale with the ring cross-section diameter, d , rather than occurring for a particular azimuthal mode number. This hypothesis is supported by the observation from the iso-surface plot of the regular mode III wake, clearly showing that the location of non-axisymmetry in the wake coincides with the recirculation zone located directly downstream of the ring cross-section.

Landau constants measured over the aspect ratio range $0 \leq Ar \leq 4$ increase in magnitude with increasing aspect ratio, from $c = -0.55$ at $Ar = 0$ to $c = -9.9$ at $Ar = 4$. The values determined as $Ar \rightarrow 0$ were shown to approach the accepted value of the Landau constant for the Hopf transition in the wake of a sphere.

7. Acknowledgments

The authors wish to thank both the Victorian Partnership for Advanced Computing (VPAC) and the Australian Partnership for Advanced Computing (APAC) consortia for providing access to the computational resources necessary to complete this study.

The support of the Australian Research Council (ARC) through a Large Grant and an International Linkage Grant is gratefully acknowledged.

The financial assistance of the Australian Postgraduate Award is gratefully acknowledged by Gregory Sheard.

References

- [1] T. Leweke, M. Provansal, The flow behind rings: bluff body wakes without end effects, *J. Fluid Mech.* 288 (1995) 265–310.
- [2] G.J. Sheard, M.C. Thompson, K. Hourigan, A numerical study of bluff ring wake stability, in: *Proceedings of the 14th Australasian Fluid Mechanics Conference*, Department of Mechanical Engineering, University of Adelaide, December, 2001.
- [3] G.J. Sheard, M.C. Thompson, K. Hourigan, On axisymmetric bluff body wakes: three-dimensional wake structures and transition criticality of the torus, in: *Proceedings of the 3rd Conference on Bluff Body Wakes and Vortex Induced Vibrations*, Port Douglas, Australia, December, 2002.
- [4] M.C. Thompson, K. Hourigan, J. Sheridan, Three-dimensional instabilities in the wake of a circular cylinder, *Exp. Therm. Fluid Sci.* 12 (1996) 190–196.
- [5] M.C. Thompson, T. Leweke, M. Provansal, Kinematics and dynamics of sphere wake transition, *J. Fluids Structures* 15 (2001) 575–585.
- [6] P. Le Gal, A. Nadim, M.C. Thompson, Hysteresis in the forced Stuart–Landau equation: application to vortex shedding from an oscillating cylinder, *J. Fluids Structures* 15 (2001) 445–457.
- [7] J. Dušek, P. Fraunić, P. Le Gal, A numerical and theoretical study of the first Hopf bifurcation in a cylinder wake, *J. Fluid Mech.* 264 (1994) 59–80.
- [8] A.G. Tomboulides, S.A. Orszag, Numerical investigation of transitional and weak turbulent flow past a sphere, *J. Fluid Mech.* 416 (2000) 45–73.
- [9] T.A. Johnson, V.C. Patel, Flow past a sphere up to a Reynolds number of 300, *J. Fluid Mech.* 378 (1999) 19–70.
- [10] B. Ghidersa, J. Dušek, Breaking of axisymmetry and onset of unsteadiness in the wake of a sphere, *J. Fluid Mech.* 423 (2000) 33–69.
- [11] J. Jeong, F. Hussain, On the identification of a vortex, *J. Fluid Mech.* 285 (1995) 69–94.